Macroscopic Traffic Flow Model Calibration for Lane-free Automated Vehicle Traffic *

Ioannis Papamichail, Nicolas Schoenn-Anchling, Milad Malekzadeh, Vasileios Markantonakis, Markos Papageorgiou, *Life Fellow, IEEE*

***Abstract*— A novel traffic paradigm was recently proposed for automated vehicles. It is characterized by two integrated principles: lane-free traffic and vehicle nudging. The latter suggests that vehicles can be influenced (nudged) by other vehicles in their vicinity, even behind them. Various vehicle movement strategies have been designed for this concept that can be employed for microscopic traffic simulation. On the other hand, macroscopic models may be used to produce large-scale simulation results with low computational effort, but also to gain insights on the emerging macroscopic properties of lane-free traffic with vehicle nudging. Furthermore, macroscopic models can be used for various significant traffic engineering tasks, including estimation and control strategy design. This paper employs an ad-hoc vehicle movement strategy for Connected and Automated Vehicles (CAVs) driving in a lane-free highway environment, to produce data that can be utilized to calibrate macroscopic models. An extended version of a well-known first-order traffic flow model is calibrated to fit the data, and optimal model parameters are determined for different highway widths and different vehicle nudging levels. The traffic conditions observed in the microscopic lane-free CAV traffic are reproduced with sufficient accuracy. Highway capacity and critical density are found to increase linearly with the increase of the highway width; and further increase of the same quantities is observed for increased levels of vehicle nudging. On the other hand, free speed is independent of the highway width and increases slightly with vehicle nudging.**

I. Introduction

TrafficFluid is a recently introduced paradigm for vehicular traffic, applicable at high levels of vehicle automation and communication systems [1]. The TrafficFluid concept suggests *lane-free* traffic, whereby vehicles are not bound to fixed traffic lanes, as in conventional traffic; and *vehicle nudging*, whereby vehicles may exert a "nudging" effect on, i.e. influence the movement of, adjacent vehicles around and, in contrast to current practice, also in front of them. Vehicles in a lane-free environment do not necessarily align to form lanes but are self-organizing into dynamically changing 2-D clusters, depending on the vehicle sizes, their desired speeds, the employed vehicle movement strategies and the prevailing vehicle density, so as to maximize the available infrastructure coverage.

Designing a safe and efficient vehicle movement strategy in lane-free traffic is a challenging problem. Various methodological approaches can be explored to achieve this objective, including strategies based on optimal control [2], non-linear feedback control [3], as well as multi-agent systems [4]. For quick verification and demonstration of the TrafficFluid concept, an ad-hoc vehicle movement strategy for lane-free traffic with nudging was suggested at an early stage [5], while an improved and strongly modified strategy followed [6]. All these vehicle movement strategies can be employed for microscopic traffic simulation that produces macroscopic data necessary to investigate empirically emerging macroscopic properties of the new concept. However, some of these movement strategies may require demanding computations; while macroscopic traffic flow models are usually less demanding for simulation purposes and may provide more direct insights of the macroscopic properties of lane-free traffic with nudging. They also have an analytical form, which allows for their usage for various significant traffic engineering tasks (estimation, control strategy design) beyond simulation. Before employing a traffic flow model in practical applications, it is crucial to first calibrate it using traffic data. The calibration procedure aims at appropriately specifying the model parameter values, so that the representation of the traffic flow characteristics is as accurate as the model structure allows. The calibration method typically involves the minimization of the discrepancy between the macroscopic model calculations and the traffic data, by use of proper optimization tools; see [7], [8].

Based on nonlinear-feedback vehicle movement control laws for CAVs on lane-free roads, an analytical procedure brought forth a space-time continuous second-order traffic flow macroscopic model [9]. Its solution was approximated by a nonlinear heat equation that was solved numerically [10], requiring, however, a high computational effort. In this work, a more practical approach is pursued, employing a space-time discrete macroscopic traffic flow model, which requires low computational effort. The model is an extended version of the well-known Cell Transmission Model (CTM) [11]. Specifically, CTM does not reproduce the capacity drop phenomenon, i.e. the empirical observation that, at the head of congestion, the discharge flow is reduced compared to the capacity of the road. For this reason, CTM was extended in several possible ways to enable the reproduction of capacity drop, see [12] for an overview and comparison. The extended CTM is calibrated in the present work to fit the microscopic lane-free data, and optimal model

* The research leading to these results has received funding from the European Research Council under the European Union's Horizon 2020 Programme / ERC Grant Agreement no. 833915, project TrafficFluid, see: https://www.trafficfluid.tuc.gr.

I. Papamichail, M. Malekzadeh, V. Markantonakis and M. Papageorgiou are with the Dynamic Systems and Simulation Laboratory, Technical University of Crete, Chania 73100, Greece. (Corresponding author email: ipapa@dssl.tuc.gr). Markos Papageorgiou is also with the Faculty of Maritime and Transportation, Ningbo University, Ningbo, China.

N. Schoenn-Anchling is with LICIT- Éco7, École nationale des travaux publics de l'État & Université Gustave Eiffel, 3 rue Maurice Audin, 69120, Vaulx-en-Velin, France

parameters are determined for different highway widths and different vehicle nudging levels to investigate their impact on macroscopic characteristics, including capacity, critical density, free speed and capacity drop.

In the following, the vehicle movement strategy developed in [6] is briefly reviewed in Section II. The macroscopic model to be calibrated is presented in Section III, and the model calibration procedure is outlined in Section IV. The calibration results and discussion follow in Section V, while conclusions are drawn in Section VI.

II. Vehicle Moving Strategy

As already mentioned in Section I, to demonstrate and verify the TrafficFluid concept, an ad-hoc vehicle movement strategy for lane-free traffic with vehicle nudging was developed [6]. This scheme has been implemented in TrafficFluid-Sim [13], [14], a lane-free extension of the well-known microscopic simulator SUMO [15], and is briefly outlined for completeness in what follows.

A double-double-integrator (DDI) model is used for the vehicle motion dynamics, consisting of the following two-dimensional kinematic equations that describe the vehicle position and speed

$$\begin{aligned} x(t+T) &= x(t) + v_x(t)T + 0.5 f_x(t)T^2 \\ v_x(t+T) &= v_x(t) + f_x(t)T \\ y(t+T) &= y(t) + v_y(t)T + 0.5 f_y(t)T^2 \\ v_y(t+T) &= v_y(t) + f_y(t)T \end{aligned} \tag{1}$$

for $t = 0, T, 2T, \ldots$ Thus, at the beginning of each time-step t of length T, each vehicle departs from position $(x(t), y(t))$, which characterizes the longitudinal and lateral coordinates of the center of the rectangular vehicle, with longitudinal (lateral) speed $v_x(t)$ $(v_y(t))$; and, moving with constant longitudinal (lateral) acceleration $f_x(t)$ $(f_y(t))$, it reaches its updated state (position and speeds) at time $t+T$. In the above set of equations, the acceleration value is a control input to be specified by the moving strategy. This model is deemed appropriate for vehicle movement that does not involve strong turnings, as is typically the case on highways.

In the employed vehicle movement strategy, longitudinal (x-direction) and lateral (y-direction) accelerations for each CAV at time t are computed via the following equations:

$$\begin{aligned} f_x(t) &= \sigma_x^{ts} f_x^{ts}(t) + f_x^{rp}(t) + \sigma^{ng} \gamma_x f_x^{ng}(t) \\ f_y(t) &= f_y^{ts}(t) + f_y^{rp}(t) + \sigma^{ng} \gamma_y f_y^{ng}(t) \end{aligned} \tag{2}$$

A brief account of the function of each "force" on the right-hand side of (2) is provided here:

- The *target-speed forces* f_x^{ts} and f_y^{ts} aim for the vehicle to attain its respective longitudinal and lateral target speeds. f_x^{ts} is active conditionally, depending on the states of the ego vehicle and of other vehicles in the vicinity. Activation or deactivation of f_x^{ts} is performed using the binary variable $\sigma_x^{ts} \in \{0,1\}$.

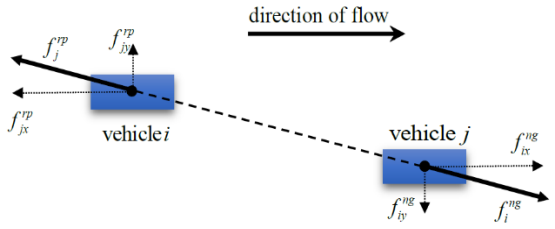

Figure 1. Visualization of repulsive and nudging forces between two vehicles.

- The *repulsive forces* f_x^{rp} and f_y^{rp} are present to prevent any crashes with vehicles ahead (downstream).
- The *nudging forces* f_x^{ng} and f_y^{ng} are present due to vehicles behind (upstream) and may facilitate advancement of faster vehicles behind, but have also an impact on the macroscopic characteristics of the emerging traffic flow [16], as also demonstrated in this paper. The coefficients $\gamma_x, \gamma_y \in [0,1]$ regulate the magnitude of nudging forces versus repulsive forces, enabling reduction of nudging forces if desired. The nudging forces f_x^{ng} and f_y^{ng} may, under circumstances, be de-activated, and this is performed using the binary variable $\sigma^{ng} \in \{0,1\}$.

Fig. 1 visualizes repulsive and nudging forces between two adjacent vehicles i and j in lane-free traffic. A repulsive force f_j^{rp} is created for each couple of adjacent vehicles, with a direction along the line connecting both vehicle centers. The repulsive force indicates towards, and applies to, the vehicle i, whose center is farther upstream. Its magnitude depends on the distance, relative speed and lateral displacement of both vehicles and is partly inspired by lane-based car-following ACC (Adaptive Cruise Control) laws. The downstream vehicle j receives a nudging force f_i^{ng} with opposite direction and equal magnitude to the repulsive force f_j^{rp}, which, however, can be moderated by the choice of the aforementioned parameters γ_x, γ_y.

The total repulsive force f^{rp}, acting on a reference vehicle, equals the sum of the strongest-in-magnitude individual repulsive forces due to vehicles within a downstream longitudinal distance. Similarly, the nudging force f^{ng}, acting on a reference vehicle, equals the sum of the strongest-in-magnitude individual nudging forces due to vehicles within an upstream longitudinal distance. After f_x and f_y have been produced from the respective sums of target-speed, repulsive and nudging forces via (2), a constraining mechanism is applied before they are used as accelerations. In particular, in order to keep a vehicle within the boundaries of the highway, lateral acceleration bounds are computed through a regulation problem, whereby a (left or right) road boundary is considered as a reference lateral position, and a lateral acceleration of the vehicle is obtained via a boundary feedback controller, such that the vehicle moves asymptotically towards the boundary, or remains on the boundary, without violating it. Consequently, such an acceleration can be used as a lateral acceleration bound to ensure that the vehicle will never cross the corresponding

road boundary. Other bounds are applied as well, e.g. to avoid the backward moving of vehicles, to avoid speeds that exceed excessively the desired (target) speeds, etc.

A comprehensive explanation of the relations leading to the aforementioned forces can be found in [6]. The simulation results presented in that work considered a ring-road without any on-ramps or off-ramps. However, to study the effect of congestion creation due to merging and the related spillback caused, the present work considers the presence of on-ramps and off-ramps, and therefore, the moving strategy must be appropriately extended compared to [6]. Specifically, while vehicles travelling on the mainstream have zero lateral target (desired) speed, vehicles travelling towards a deceleration lane that leads to an off-ramp; or vehicles travelling on an on-ramp and trying to merge to the mainstream through an acceleration lane are assigned a negative or a positive desired lateral speed, respectively, to enable corresponding smooth exiting or entering maneuvers. On the top of these, to further ensure that the exiting or entering vehicles remain within the extended road boundaries of the acceleration and deceleration lanes, appropriate additions to the aforementioned feedback boundary controller are introduced.

III. Macroscopic Model

The macroscopic model considered for calibration is an extended version of CTM [12] that includes terms allowing for the reproduction of the capacity drop phenomenon. The same model has been used for the formulation of optimal control problems, feedback control design as well as macroscopic simulations for lane-free automated vehicle traffic [17], [18].

A highway stretch is considered (see Fig. 4 as an example) that is subdivided into n sections (or cells) with lengths L_i, $i=1,2,\dots,n$. The conservation equation for each section is given by

$$\begin{aligned}\rho_1(k+1) &= \rho_1(k)+\frac{T_m}{L_i}(q_0(k)-q_1(k))\\ \rho_i(k+1) &= \rho_i(k)+\frac{T_m}{L_i}((1-\beta_i)q_{i-1}(k)-q_i(k)+r_i(k)),\quad (3)\\ i &= 2,3,\dots,n\end{aligned}$$

where T_m is the model time-step and $k=0,1,\dots,K-1$ is the corresponding discrete-time index. ρ_i (in veh/km) and q_i (in veh/h) denote, respectively, the traffic density and the mainstream exit flow of section i. Thus, q_0 (in veh/h) is mainstream demand. Every section, except for the most upstream, may have an on-ramp or an off-ramp at its upstream boundary. The on-ramp flow (if any) at section i is denoted r_i (in veh/h), while the off-ramp flow (if any) of section i is calculated based on known exit rates β_i multiplied with the upstream-section flow, i.e. $\beta_i q_{i-1}$.

The movement of vehicles from one cell to the next is governed by the steady-state relation between flow and density, i.e. the Fundamental Diagram (FD). Traffic flow is obtained as the minimum of demand and supply functions Q_D and Q_S, except for the last section, where only the demand function is considered, assuming that the downstream traffic conditions are uncongested. Specifically, we have

$$\begin{aligned}q_i(k) &= \min\left\{Q_{D,i}(\rho_i(k)),\frac{Q_{S,i+1}(\rho_{i+1}(k))}{(1-\beta_{i+1})}-\lambda_r r_{i+1}(k)\right\},\\ &\quad i=1,2,\dots,n-1\\ q_n(k) &= Q_{D,n}(\rho_n(k)).\end{aligned}\quad (4)$$

According to the original CTM [11], a triangular-shaped FD is considered, hence the demand and supply functions are given by the following respective equations

$$\begin{aligned}Q_{D,i}(\rho) &= \min\left\{q_{cap,i}+\lambda_d q_{cap,i}\frac{\rho-\rho_{cr,i}}{\rho_{cr,i}-\rho_{\max,i}},v_{f,i}\rho\right\},\\ Q_{S,i}(\rho) &= \min\left\{q_{cap,i},w_{s,i}(\rho_{\max,i}-\rho)\right\},\end{aligned}\quad (5)$$

where $v_{f,i}$ (in km/h) is the free speed of a section i, $q_{cap,i}$ (in veh/h) is the section capacity achieved for density equal to the critical density $\rho_{cr,i}$, i.e. $q_{cap,i}=v_{f,i}\rho_{cr,i}$, $w_{s,i}$ (in km/h) is the back-wave speed and $\rho_{\max,i}$ (in veh/km) is the jam density, while $q_{cap,i}=w_{s,i}(\rho_{\max,i}-\rho_{cr,i})$ and $w_{s,i}<v_{f,i}<L_i/T$. Furthermore, the option of introducing capacity drop trough appropriate terms, according to Approach 5 presented in [12], is incorporated in the above equations. More specifically, this option is enabled via the global parameters λ_r and λ_d in equations (4) and (5). If these parameters are set to $\lambda_r=1$ and $\lambda_d=0$, no capacity drop is reproduced, as typical for the original CTM; if these parameters are set to $\lambda_r<1$ and $\lambda_d>0$, a corresponding level of capacity drop is produced by the model. This approach allows for the bottleneck (e.g. merge) section to become congested (as in real traffic) by allowing more flow (than with the original CTM) to enter the section, while producing a reduced outflow as well.

The model presented above includes a few parameters, whose values may differ for different highway sites and depend on factors such as highway geometry, driver behavior (in case of manually driven vehicles) or moving strategy used (in case of automated traffic), distribution of vehicle sizes, weather conditions etc. The reliability and accuracy of the model rely on the appropriate specification of its parameter values. Therefore, calibration of the model is required before using it. At the same time, separate model calibration under varying conditions (e.g. different highway widths or of nudging factor strengths) may reveal highly interesting aspects and properties of lane-free traffic considered here.

IV. Model Calibration Procedure

The model calibration (or parameter estimation) procedure aims at enabling a macroscopic traffic flow model to represent traffic conditions of a highway stretch with the highest possible accuracy. This procedure has been

described in the past, e.g. see [8], and is outlined here for completeness. The estimation of the unknown model parameters is not a trivial task since the system equations are usually highly nonlinear. It should be highlighted that, in the present context, another major motivation for model calibration is to study the emerging features and properties of lane-free traffic at the macroscopic level under several infrastructure (road width) and microscopic movement (nudging) conditions.

Consider that a macroscopic discrete-time state-space model is described by the following state equation

$$\begin{aligned} &\mathbf{x}(k+1) = f(\mathbf{x}(k), \mathbf{d}(k), \mathbf{p}), \quad k = 0,1,\ldots,K-1 \\ &\mathbf{x}(0) = \mathbf{x}_0 \end{aligned} \tag{6}$$

where $\mathbf{x}$ is the state vector, $\mathbf{d}$ is the external variable vector and $\mathbf{p}$ is the parameter vector. The extended CTM presented above can readily assume the state space form of (6) for any highway stretch. In particular, the state vector $\mathbf{x}$ includes the section densities, the external variable vector $\mathbf{d}$ consists of the mainstream and on-ramp inflows and the turning rates at the off-ramps; and $\mathbf{p}$ holds the unknown model parameters that need to be specified.

If the initial state $\mathbf{x}_0$ is given and the external vector $\mathbf{d}(k)$ is known over a time horizon $k = 0,1,\ldots,K-1$, then the model (6) may be run to produce all states. The parameter estimation problem can be formulated as a nonlinear least-squares output error problem which aims at the minimization of the discrepancy between the model output and the corresponding traffic measurements by use of the following cost function

$$J(\mathbf{p}) = \sum_{k \in M} \left\| \mathbf{y}(k) - \mathbf{y}^m(k) \right\|_{\mathbf{Q}}^2 \tag{7}$$

subject to (6), where $\mathbf{Q}$ is a positive definite diagonal matrix, $\mathbf{y}(k) = \mathbf{g}(\mathbf{x}(k))$ is the measurable model output vector (typically including flows and mean speeds at different sections of the highway) and $\mathbf{y}^m(k)$ includes the measured traffic data, consisting of flows and speeds at the corresponding locations. Also, $M \subseteq \{1,2,\ldots,K\}$, i.e. the M set may be a subset comprising only some simulation steps, since the simulation time step (e.g. $T_m = 10$ s) is usually smaller than the measurements interval (e.g. 60 s).

The parameter values for the model are selected from a closed admissible region of the parameter space, which is determined via physical considerations and experience. Finding the optimal parameter set requires an appropriate nonlinear programming routine, whereby for each choice of a new parameter vector $\mathbf{p}$, the value of the cost function (7) may be computed by a run of the model equations as shown in Fig. 2; the routine attempts in subsequent iterations to improve the cost function, until a local minimum is reached.

The nonlinear, non-convex least-squares optimization problem of parameter estimation is known to have multiple local minima, and hence gradient-based optimization algorithms are not appropriate. Previous studies have

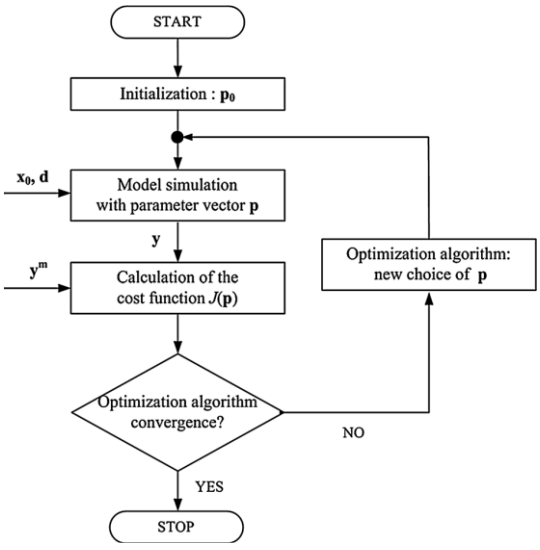

Figure 2. Model calibration procedure [8].

utilized various derivative-free optimization algorithms to solve the parameter estimation problem. Three derivative-free optimization algorithms are compared in [8] to investigate which is more suitable for the problem. In particular, the deterministic Nelder-Mead algorithm [19], [20], a stochastic genetic algorithm [21], and the stochastic cross-entropy method [22] were used. The optimization results showed that all three algorithms converge to robust model parameter sets, albeit achieving different performances considering the required computation time, with the Nelder-Mead algorithm outperforming the rest.

The Nelder-Mead algorithm makes use of a simplex; every vertex of the simplex corresponds to a potential solution which in turn corresponds to a cost function value. The algorithm starts with an initial simplex and then performs a sequence of transformations aiming at reducing the worst cost function value among its vertices. Simplex transformations are controlled by four parameters: ζ for reflection, χ for contraction, γ for expansion and σ for shrinkage.

The CALISTO software tool is a Matlab implementation of the model calibration procedure described above [23]. This implementation is able to perform calibration of different discrete-time models (CTM [11], METANET [24], as well first-order traffic flow models incorporating capacity drop [12]) using different optimization algorithms. This tool has been recently implemented in C to reduce computational time and was used to produce the calibration results presented in the following section for the extended CTM utilizing the Nelder-Mead algorithm.

V. Calibration Results and Discussion

A. Simulation Set-up and Traffic Data Generation

Numerous microscopic simulations, each having a duration of 1 h, were designed and carried out by use of the ad-hoc vehicle movement strategy presented in Section II, implemented in TrafficFluid-Sim (see Fig. 3), to generate

the macroscopic traffic data necessary to calibrate the macroscopic traffic flow model. The vehicle movement strategy is employed with a time step equal to 0.2 s for simulation on a highway stretch of 5 kilometers in length that includes an on-ramp and an off-ramp. A sketch of the highway stretch is presented in Fig. 4. The stretch is divided into 10 sections (S1-S10), with a length of 500 m each, that match the sections to be used for the macroscopic model. Outflow and mean speed measurements were collected every 10 s for each section, to be used for comparison with the macroscopic model results in the objective function.

The dimensions of the vehicles are determined by choosing randomly (with uniform distribution) one out of the six "dimension classes" reported in Table I. Also, the desired longitudinal speed assigned to a vehicle is chosen randomly (with uniform distribution) within the range [25, 35] m/s = [90, 126] km/h.

Lane-free traffic is deemed to imply that incremental changes of the road width may lead to corresponding incremental changes of capacity. This is because lane-free driving vehicles may spread and exploit any portion of additional road width, even if it is much less than a whole conventional traffic lane. Based on this assumption, IBC (Internal Boundary Control), a novel control measure for lane-free CAV traffic, was proposed and tested macroscopically in [17], [18]. To investigate microscopically the validity of that assumption, i.e. to investigate the impact of the highway width on the parameters of the macroscopic model, separate simulations are performed for different widths, starting from a nominal width of 10.2 m (corresponding to the width of 3 conventional lanes) and widening or narrowing it by multiples of 0.85 m (corresponding to the width of one quarter of a conventional lane). As the highway capacity is expected to increase (decrease) for wider (narrower) widths, different mainstream demand profiles are used per width, increased (decreased) compared to the one utilized for the nominal width, to ensure that the bottleneck at the merging area is activated for a period of time, causing congestion that spills back for a few sections of the highway. This is necessary in order to have calibration data that span the whole spectrum of possible traffic conditions, including free flow, critical and congested traffic conditions.

Furthermore, it is interesting to investigate and demonstrate the impact of different values for the coefficients γ_x, γ_y that regulate the influence of nudging forces. To this end, the following three cases were considered:

- No nudging forces applied $(\gamma_x = 0, \gamma_y = 0)$;
- Weak nudging forces applied $(\gamma_x = 0.5, \gamma_y = 0.5)$;
- Nominal (full) nudging forces applied $(\gamma_x = 1, \gamma_y = 1)$.

TABLE I. THE DIFFERENT DIMENSION CLASSES OF VEHICLES USED IN THE SIMULATION EXPERIMENT.

	Class 1	Class 2	Class 3	Class 4	Class 5	Class 6
Length (m)	3.20	3.90	4.25	4.55	4.60	5.15
Width (m)	1.60	1.70	1.80	1.82	1.77	1.84

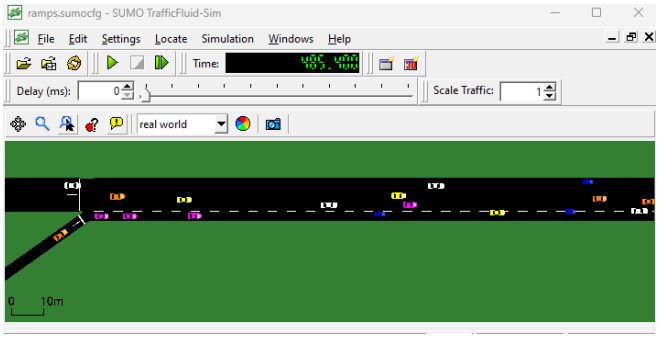

Figure 3. A snapshot of the simulation environment TrafficFluid-Sim.

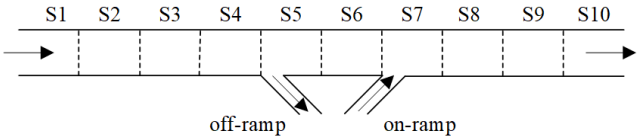

Figure 4. A sketch of the highway stretch used for the simulations.

The mainstream demand used is slightly higher in case of vehicle nudging, as a capacity increase is expected. All the other parameters used for the ad-hoc vehicle movement strategy are as in [6].

B. *Calibration Problem Parameters*

After generating the macroscopic data via microscopic simulation, the calibration procedure can be applied using CALISTO. The extended CTM time-step used is 10 s, i.e. equal to the measurement step. Since the highway stretch considered is small and there are no changes in geometry for the highway sections, it is assumed that the model parameters used within the demand and supply functions are the same for all sections. Five model parameters are optimized, namely the free speed v_f, the capacity q_{cap}, the back-wave speed w_s and the capacity drop parameters λ_r and λ_d. The other two parameters, i.e. the critical density ρ_{cr} and the jam density $\rho_{\max}$, can be calculated using the values of the optimization parameters as $\rho_{cr} = q_{cap} / v_f$ and $\rho_{\max} = q_{cap} / w_s + \rho_{cr}$. The macroscopic model used delivers directly densities ρ_i and flows q_i for each section i; and as it is a first-order model, the mean speed for each section i (to be used in the model output vector) is taken as q_i / ρ_i.

The diagonal elements of the diagonal matrix $\mathbf{Q}$, used in the cost function (7), that correspond to speed are set to 1, while those that correspond to flow are set to 10^{-2}. The Nelder-Mead algorithm was employed using the following parameters: $\zeta = 1$, $\chi = 2$, $\gamma = 0.5$ and $\sigma = 0.5$. Its parameterization was based on various initial calibration tests and previous experience. Moreover, the utilized termination criteria are the cost function convergence or the working simplex convergence; and the maximum allowed number of iterations was set to 2000.

C. *Results and Discussion*

The demand trajectories used for the case of nominal highway width of 10.2 m and full nudging are presented in Fig. 5, while the space-time diagrams of measured

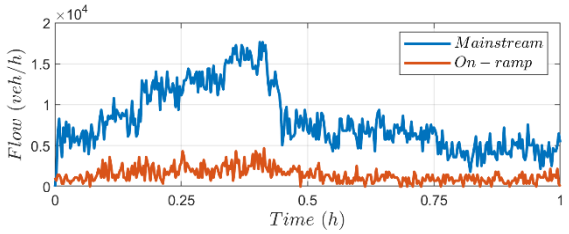

Figure 5. Mainstream and on-ramp demand trajectories used for highway width of 10.2 m and full nudging.

(microscopically simulated) mean speed and flow are depicted in Fig. 6 (left column). It can be observed that during the pick of the demand, the merging area bottleneck at section 7 (S7) is activated, at around $t = 0.4$ h, and congestion is created that spills back and covers a couple of upstream sections. The corresponding space-time diagrams of the macroscopic model values of speed and flow, after calibration, are depicted in Fig. 6 (right column) and demonstrate that the traffic conditions appearing with microscopic lane-free automated vehicle traffic are reproduced with reasonable accuracy by the calibrated macroscopic traffic flow model. Fig. 7 presents trajectories for the measured bottleneck outflow and the corresponding macroscopic model estimate. The obtained fit is very good and the capacity drop, observed in the data of the microscopic simulation at around $t = 0.4$ h at the head of the congestion, is reproduced by the macroscopic model.

The calibrated capacity values obtained for different highway widths and different nudging strengths are presented in Fig. 8 (upper). It is clear that capacity increases with increasing highway width. It is also clear that capacity increases with increasing vehicle nudging strength for any width. In more quantitative terms, the same figure displays the lines produced via linear regression without the intercept term, i.e. assuming that the capacity is analogous to the width, for each nudging case. The resulting values for the coefficient of determination r^2 are 0.95, 096 and 0.98 for the full nudging, weak nudging, and no nudging cases, respectively. This excellent match underlines and verifies the conjecture expressed in [17], [18] in the context of IBC, namely that the capacity of the highway in lane-free CAV driving depends linearly and continuously on the road width, which implies that any incremental width change leads to an analogous capacity change. In addition, in the present investigation, the capacities reached are about 2 to 2.5 times higher than the capacity observed on a highway with conventional lanes, depending on the nudging strength. The regression lines have the form $q_{cap} = a \cdot w$, where w is the highway width in meters and a equals 1322 veh/h/m for no nudging, 1538 veh/h/m for weak nudging and 1681 veh/h/m for full nudging. Thus, in the present investigations, weak nudging increases the capacity by $(1538 - 1322)/1322 = 16.3\%$; and full nudging increases the capacity by $(1681 - 1322)/1322 = 27.2\%$.

On the other hand, the calibrated free speed does not

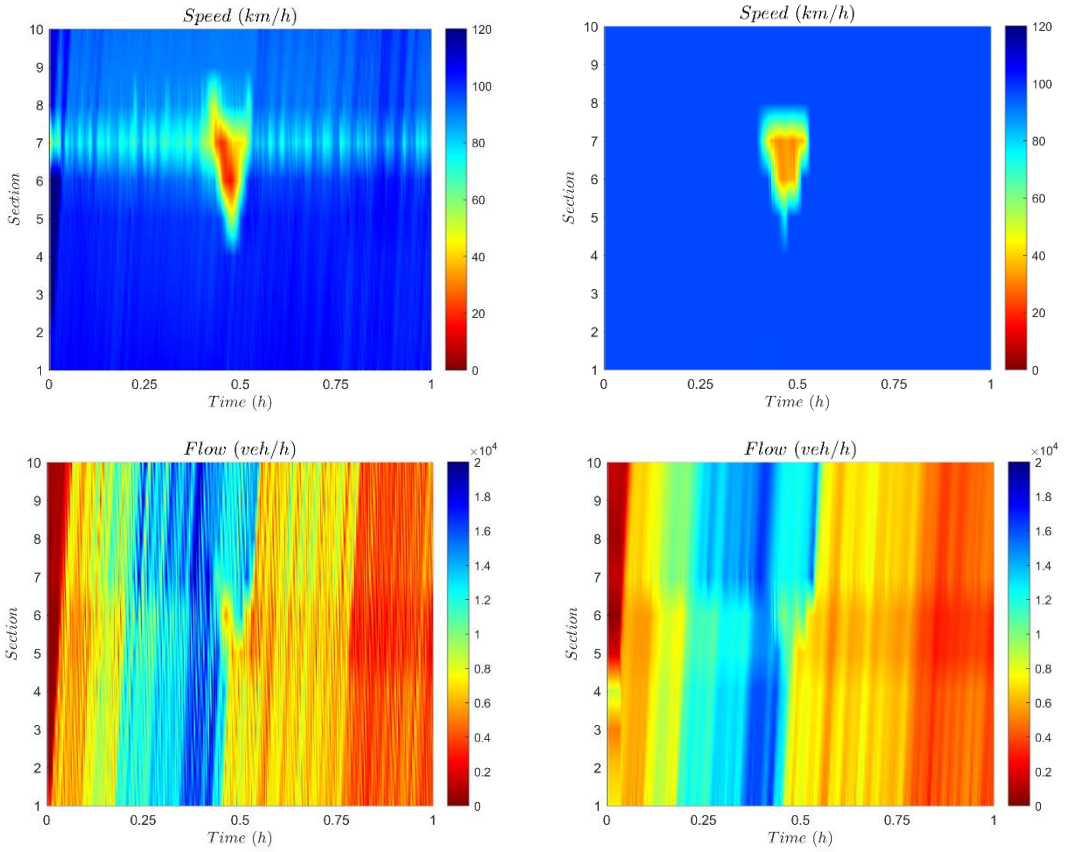

Figure 6. Space-time diagrams of microscopically produced speed and flow (left column) versus macroscopic model estimates (right column) for highway width of 10.2 m and full nudging

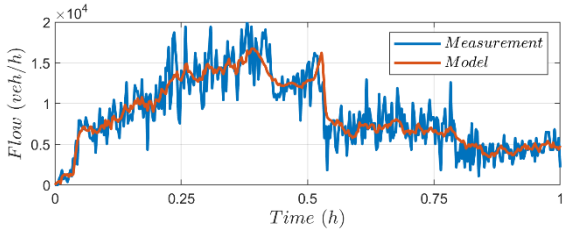

Figure 7. Bottleneck (section 7) outflow measurement trajectory and macroscopic model estimate for highway width of 10.2 m and full nudging.

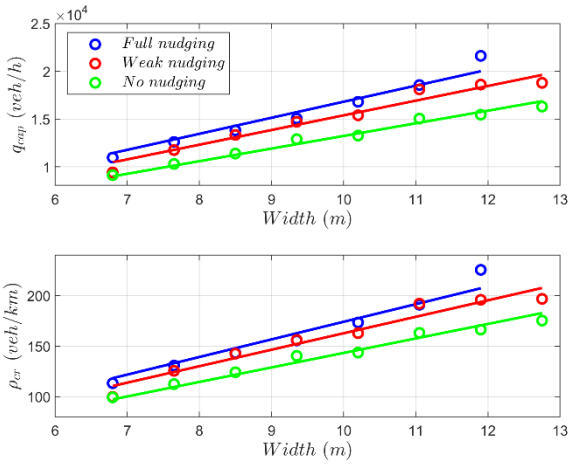

Figure 8. Capacity (upper) and critical density (lower) versus highway width for full, weak and no nudging.

depend on the width of the highway, something that is consistent with the assumptions in [17], [18] and is physically comprehensible, since road widening does not affect the desired speeds of vehicles nor the way vehicles interact with each other at near-critical densities. Thus, the free speed is found to be almost constant in dependence of the highway width. Regarding nudging, the calibrated free speed has an average value of 96.6 km/h, 94.3 km/h and 92.1 km/h for the full nudging, weak nudging, and no nudging cases, respectively. This indicates a slight dependence of free speed on nudging strength, which can also be physically justified by the fact the nudging increases the speed of interacting vehicles at near-critical densities.

As a consequence of linearly increasing capacity and constant free speed, in dependence of the highway width, in a triangular fundamental diagram, the critical density, calculated from the calibrated values of capacity and free speed, must also depend linearly on the highway width; and increase for increased levels of nudging, as is indeed shown in Fig. 8 (lower). The values for the coefficient of determination r^2 are, for the critical density, similarly high as for capacity, amounting to 0.95, 095 and 0.97 for the full nudging, weak nudging, and no nudging cases, respectively. Again, this is in close agreement with the assumption made in [17], [18], where the same extended CTM was used for the formulation of optimal control problems, feedback control design and macroscopic simulations, all for lane-free automated vehicle traffic.

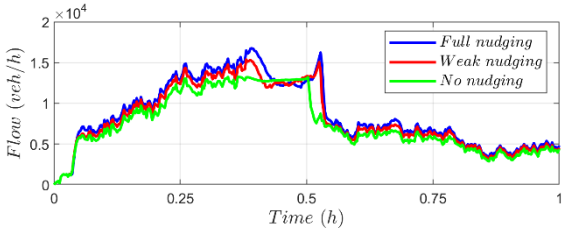

Figure 9. Macroscopic model trajectories of outflow at the bottleneck (section 7) for highway width of 10.2 m and for full, weak and no nudging.

When it comes to the calibrated back-wave speed values, and the resulting jam density values, the results are rather inconclusive. The first observation is that the estimated values for the back-wave speed are large compared to the values known for conventional traffic. Also, one would expect the back-wave speed to be constant so as to have a jam density that depends linearly on the highway width. However, this is not the case. Thus, this outcome is not conform with the conjecture in [17], [18], but is of less importance compared to the aforementioned findings regarding capacity, critical density and free speed. In fact, this discrepancy is attributed to the absence of heavily congested states in the microscopic simulation, because of which the calibration procedure, while reproducing reasonably well the measurements, has a difficulty to identify the exact values of the involved macroscopic parameters of back-wave speed and jam density. More investigations with larger and different simulation data sets are needed, containing heavier congestion for longer periods of time covering larger areas of the highway stretch. This, along with possible fixes in the calibration procedure, may improve the identifiability of the back-wave speed and jam density, leading to more reliable parameter estimates. Another possible way of achieving this is by increasing the diagonal elements of the matrix $\mathbf{Q}$, used in the cost function (7), that correspond to speed and flow differences for the sections that are affected by congestion.

Regarding the important issue of capacity drop, the relevant parameters are λ_r and λ_d, see (4) and (5). On average, the obtained value for λ_r is -0.33, which means that the merge area is allowed to become congested by letting more flow to enter this section due to the increased supply term considered when deciding on the outflow of the upstream section. Also, on average, the obtained value for λ_d, is 0.4, which means that the merge area outflow is reduced compared to the capacity value that would otherwise prevail for the original CTM. Most importantly, the capacity drop observed in the data is very well reproduced, see Fig. 7. Also, as can be seen in Fig. 9, although capacity is increasing with increased vehicle nudging, the discharge flow rate remains equal for all nudging strengths. As a result, capacity drop is increasing with nudging. We have no intuitive explanation for this finding at the present stage, and more investigations are necessary for understanding the impact of nudging on discharge flow and capacity drop.

VI. Conclusion

Lane-free automated vehicle traffic has recently been proposed and studied using various vehicle movement strategies. Microscopic simulations with these strategies can produce macroscopic data that are useful to investigate empirically the emerging macroscopic properties of the new concept. An ad-hoc lane-free vehicle movement strategy was used in this paper to produce data for a highway stretch with one on-ramp and one off-ramp. Subsequently, a macroscopic model, an extended version of CTM, was calibrated to fit the data and optimally estimated macroscopic model parameters have been determined for different highway widths and different vehicle nudging levels. The traffic conditions observed in the microscopic lane-free automated vehicle traffic were reproduced with reasonable accuracy by the calibrated macroscopic model. Also, the capacity drop, observed in the data at the head of the congestion, is adequately reproduced by the model.

Based on the calibrated values obtained for the macroscopic model parameters, the following conclusions can be drawn. Capacity increases linearly and continuously with the increase of highway width; and increases further for increased levels of vehicle nudging. Depending on the level of nudging, capacity values are about 2 to 2.5 times higher than those observed on a highway with conventional lanes. Free speed does not depend on the width of the highway; and increases slightly with vehicle nudging. As a result, critical density depends also linearly on the highway width and increases for increased level of nudging. These findings are fully consistent with the conjectures of [17], [18], based on which the novel control measure of internal boundary control was proposed, designed and tested. On the other hand, more investigations are necessary to get further insights and reliable conclusions regarding the back-wave speed and the jam density. The discharge rate at the head of congestion was found in the microscopic simulations to be independent of the nudging strength; as a consequence, capacity drop is found to increase with vehicle nudging. Despite some uncertainties in the values and role of some macroscopic model parameters, at a phenomenological level the calibrated macroscopic model matched well the discharge flow and capacity drop produced in the lane-free simulation. More investigations are necessary for better understanding of some issues related to discharge flow, capacity drop and macroscopic model parameters. Future work will also include calibration of other first-order as well as second-order macroscopic traffic flow models for lane-free traffic with nudging.

References

[1] M. Papageorgiou, K.S. Mountakis, I. Karafyllis, I. Papamichail, and Y. Wang, "Lane-free artificial-fluid concept for vehicular traffic," *Proceedings of the IEEE*, vol. 109, no. 2, pp. 114-121, 2021.

[2] V.K. Yanumula, P. Typaldos, D. Troullinos, M. Malekzadeh, I. Papamichail, and M. Papageorgiou, "Optimal trajectory planning for connected and automated vehicles in lane-free traffic with vehicle nudging," *IEEE Transactions on Intelligent Transportation Systems*, vol. 8, pp. 2385-2399, 2023.

[3] I. Karafyllis, D. Theodosis, and M. Papageorgiou, "Lyapunov-based two-dimensional cruise control of autonomous vehicles on lane-free roads," *Automatica*, Vol. 145, Article 110517, 2022.

[4] D. Troullinos, G. Chalkiadakis, I. Papamichail, and M. Papageorgiou, "Collaborative multiagent decision making for lane-free autonomous driving". In *Proceedings of the 20th International Conference on Autonomous Agents and MultiAgent Systems*, 2021, pp. 1335-1343.

[5] M. Papageorgiou, K.S. Mountakis, I. Karafyllis, and I. Papamichail, "Lane-free artificial-fluid concept for vehicular traffic," 2019, arXiv preprint arXiv:1905.11642.

[6] M. Malekzadeh, D. Manolis, I. Papamichail, and M. Papageorgiou, "Empirical investigation of properties of lane-free automated vehicle traffic," In *25th IEEE International Conference on Intelligent Transportation Systems (ITSC 2022)*, pp. 2393-2400, 2022.

[7] M. Treiber and A. Kesting, *Traffic flow dynamics*. Berlin: Springer, 2013.

[8] A. Spiliopoulou, I. Papamichail, M. Papageorgiou, Y. Tyrinopoulos, and J. Chrysoulakis, "Macroscopic traffic flow model calibration using different optimization algorithms," *Operational Research: An International Journal*, vol. 17, pp. 145-164, 2017.

[9] I. Karafyllis, D. Theodosis, and M. Papageorgiou, "Constructing artificial traffic fluids by designing cruise controllers," *Systems & Control Letters*, vol. 167, Article 105317, 2022.

[10] D. Theodosis, I. Karafyllis, G. Titakis, I. Papamichail, and M. Papageorgiou, "Performance evaluation of cruise-controlled vehicles on a macroscopic scale," *Mediterranean Conference on Control and Automation (MED 2023)*, Limassol, Cyprus, June 26-29, 2023.

[11] C.F. Daganzo, "The cell transmission model: A dynamic representation of highway traffic consistent with the hydrodynamic theory," *Transportation Research Part B*, vol. 28, pp. 269-287, 1994.

[12] M. Kontorinaki, A. Spiliopoulou, C. Roncoli, and M. Papageorgiou, "First-order traffic flow models incorporating capacity drop: Overview and real-data validation," *Transportation Research Part B*, vol. 106, pp. 52-75, 2017.

[13] D. Troullinos, G. Chalkiadakis, D. Manolis, I. Papamichail, and M. Papageorgiou, "Lane-free microscopic simulation for connected and automated vehicles," In *2021 IEEE International Intelligent Transportation Systems Conference (ITSC)*, pp. 3292-3299, 2021.

[14] D. Troullinos, G. Chalkiadakis, D. Manolis, I. Papamichail, and M. Papageorgiou, "Extending SUMO for lane-free microscopic simulation of connected and automated vehicles," In *SUMO Conference Proceedings*, vol. 3, pp. 95-103, 2022.

[15] P.A Lopez, M. Behrisch, L. Bieker-Walz, J. Erdmann, Y.P. Flötteröd, R. Hilbrich, L. Lücken, J. Rummel, P. Wagner, and E. Wießner, "Microscopic traffic simulation using sumo," In *2018 21st International Conference on Intelligent Transportation Systems (ITSC)*, pp. 2575-2582, 2018.

[16] I. Karafyllis, D. Theodosis, and M. Papageorgiou. "Analysis and control of a non-local PDE traffic flow model," *International Journal of Control*, vol. 95, pp. 660-678, 2022.

[17] M. Malekzadeh, I. Papamichail, M. Papageorgiou, and K. Bogenberger, "Optimal internal boundary control of lane-free automated vehicle traffic," *Transportation Research Part C*, vol. 126, Article 103060, 2021.

[18] M. Malekzadeh, I. Papamichail, and M. Papageorgiou, "Linear-Quadratic regulators for internal boundary control of lane-free automated vehicle traffic," *Control Engineering Practice*, vol. 115, Article 104912, 2021.

[19] J.A. Nelder and R. Mead, "A simplex method for function minimization," *Computer Journal*, vol. 7, pp. 308-313, 1965.

[20] J.C. Lagarias, J.A. Reeds, M.H. Wright, and P.E. Wright, "Convergence properties of the Nelder–Mead simplex method in low dimensions," *SIAM Journal on Optimization*, vol. 9, pp. 112-147, 1998.

[21] D. Goldberg, *Genetic algorithms in search, optimization and machine learning*, Reading: Addison-Wesley Professional, 1989.

[22] R.Y. Rubinstein and D.P. Kroese, *The cross-entropy method: a unified approach to combinatorial optimization, Monte-Carlo simulation, and machine learning*. New York: Springer, 2004.

[23] A. Spiliopoulou, I. Papamichail, M. Papageorgiou, and J. Chrysoulakis, *CALISTO user's manual*, Deliverable 4.1, Technical Report for the Project SMOOTH, ARCHIMEDES III, Athens, 2014.

[24] A. Messmer and M. Papageorgiou, "METANET: a macroscopic simulation program for motorway networks," *Traffic Engineering & Control*, vol. 31, pp. 466-470, 1990.